BACHELOR

The influence of buffer conditions on the capturing of nano-sized targets using microparticles

Hijnen, K.

Award date:
2011

The influence of buffer conditions on the capturing of nano-sized targets using microparticles

K. Hijnen
MBx 2011-10

Supervisors
A. van Reenen and
A.M. de Jong

Abstract

In this report the capture of nano-sized biotin coated fluorescent particles by streptavidin coated microparticles is studied as a model system for target capture in low concentration biosensing. The effect of different buffer conditions on the reaction kinetics is quantified. The conditions that were varied in the experiments are the ionic strength (varied with PBS concentration) and the concentration of blocking agent BSA. Also, the effect of mixing on the capturing process is evaluated.

It is found that the presence of ions in the solution causes shielding of the electrostatic charge of the particles. Increased shielding allows particles which are either negatively or positively charged to approach each other more closely, resulting in an increased rate of bond formation. At physiological conditions, the repulsive electrostatic interaction is screened for 96%.

Comparing particle capture by means of diffusive transport, i.e. applying no fluid agitation, to active fluid agitation by vortex mixing, it was found that even for low ionic strengths, particle binding is still possible. From this it followed that a low ionic strength does not significantly affect the reactivity of the particles. In addition it was found that active fluid agitation increased the reaction rate constant with a factor in the order of 10^4.

No connection was found when comparing the capturing processes in buffer solutions containing different concentrations of blocking agent BSA. Concluded was that BSA does not influence or interfere with the streptavidin-biotin bond based capturing process of the fluorescent target particles by the superparamagnetic capture particles.

Index

1. Introduction 1

2. Theory 5
2.1 Reaction kinetics 5
2.2 DLVO theory 7
2.2.1 The Van der Waals interaction 7
2.2.2 Electric double layer 8
2.2.3 The Van der Waals interaction and double layer effect combined 10

3. Experimental setup 11
3.1 Target and capture particles 11
3.2 Measurement setup 11
3.3 Measuring binding events 12
3.4 Influence of ionic strength on the reaction rate constant 15
3.5 Influence of mixing on the capturing process 15
3.6 Influence of BSA on the capturing process 15

4. Results 16
4.1 Fluorescent particle concentration correction factor 16
4.2 Influence of ionic strength on the reaction rate constant 17
4.3 Influence of mixing on the capturing process 20
4.4 Influence of BSA on the capturing process 21
4.5 Model of the interaction energy 23

5. Conclusions 25

6. References 27

Appendices 28
Appendix I – Fluorescent particle correction factor: Detailed calculations 28
Appendix II – Influence of mixing on the capturing process: Fit function 28
Appendix III – Model of the interaction energy: Parameter information 29

1. Introduction

In the ever developing field of medical sciences, the focus is on delivering excellent, efficient and reliable healthcare. A large part of healthcare consists of running diagnostic tests on samples which is often a slow process in the modern day hospital. Tests have to be approved and scheduled, working hours of lab personnel has to be taken into account, then the results need to be filed and sent to the physicians that ordered them, who in turn feed the results back to the patient at a later, pre-determined moment. This causes the patient to have to wait for days, sometimes weeks, while his or her symptoms and, more importantly, the disease are left untreated. In order to circumvent the slow processes in the hospital, it can be favorable if some (simple) tests concerning common bodily samples as blood, saliva or urine could be done outside the lab, maybe even by patients themselves. The devices that enable this are called biosensors.

Good healthcare depends on making the right decisions in sometimes urgent situations. But also, if biosensors are to be applied in daily life of patients who need regular monitoring, it is convenient test results are available on the spot. So, in contrast to the days or weeks it takes to get results in the hospital, biosensors are to be designed to deliver results in a manner of maybe hours, but preferably minutes or even seconds. To make the laboratories and its slow (administrative) processes obsolete, the results should be produced in the same place as the sample is taken. This means the biosensor should be portable, either by medical staff, paramedics or patients themselves. In the last case, portable means preferably approximately pocket-sized. As with all electronic devices, size is only diminished as technology and knowledge advances, because limiting size introduces limiting factors in the design. These include for example the choice of type of power source and considering some physical behavior changes, for example in fluid dynamics when entering the micro-sized domains. On top of that, biosensors should be easy in use, especially the models that will be used by patients. This means an easy method of collecting samples is necessary, the test procedure should be simple and the results are to be comprehendible and directly translated to a certain treatment plan. The demands mentioned above are summarized in the term “point-of-care testing”, which thus means that the device has to deliver reliable, fast and easy interpreted results on the spot.

The biosensor is relatively new product on the medical market, and therefore, the processes involved in the working principles of biosensors are an important field of study. The samples are (in the medical field) of biological nature and contain a large variety of substances from which only one specific target has to be detected and measured. If the capturing/detecting method is not sufficiently specific, the unimportant substances can cause noise in the measurement. It is also important to consider the concentration at which different substances exist in samples. If the concentration of the target is very high, some specificity and selectivity may be sacrificed in favor of the speed at which the sensor delivers results. However, if the target concentration is very low, more attention should be given to the specificity of the biosensor in order to give reliable results. Also, the properties of the target substance itself play an important role in designing the working methods in the biosensor. Thus, depending on the target substance, sample treatment and measuring methods can differ between biosensors.

A well known example of a point-of-care biosensor already in use is the glucose biosensor. Patients with diabetes have to monitor the glucose levels in their blood. A small sample of blood is put on a replaceable test strip and analyzed to determine glucose levels to see if levels are in safe ranges or that treatment (typically with an insulin injector) is needed. Released on the market in 1975 by Yellow Springs Instruments, it was the first commercial and portable biosensor that could be operated by patients themselves. Different detection and measuring techniques were applied during the evolution of the glucose biosensor to its present form. A modern day example of the glucose biosensor is shown in Figure 1a. The amount of glucose present in the sample can be measured by different methods, but generally, redox reactions are used. These are initiated by the interaction of glucose with the enzyme glucose oxidase. The reaction produces a hydrogen peroxide molecule, which in turn can take part in a redox reaction with horseradish peroxidase, absorbing an electron from the detector surface. Glucose indirectly induces a current which can be measured and related to the glucose concentration. A schematic representation of the process is given below, in Figure 1b.[1]

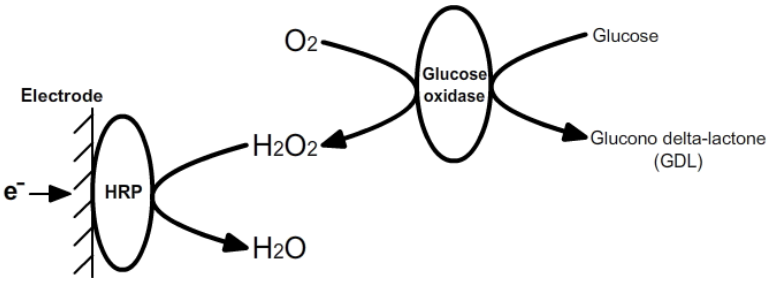

Figure 1a (left): A modern day glucose biosensor. Figure 1b (right): The schematic reaction chain in which a single glucose molecule is detected. Under influence of glucose oxidase, glucose is oxidized, forming hydrogen peroxide and GDL. The H_2O_2 then takes part in a redox reaction with horseradish peroxidase (HRP) as catalyst, using one electron, forming a current when more glucose molecules are present in the sample.

It is important to note that glucose exists in blood in relatively high concentrations, in the order of mM. Other substances are only found in much smaller concentrations, say, orders of pM, and these are therefore much harder to detect and measure. The relatively high concentration of glucose makes the detection method described above possible. The concentration is high enough for the signal to rise above the noise of detected current resulting from nonspecific interactions. However, if the concentration of the target substance is lower and comparable to other substances in the sample, this may not be the case and more specific techniques can be used. This involves actively searching the sample for the targets rather than letting them reach the detection platform by diffusion. The particles of the target substance can be specifically labeled to actively distinguish it from surrounding substances, thus increasing selectivity. Labeling is done with particles that are added to the sample which can either increase the chance of detection or be controlled actively to practically ensure detection of a labeled target particle. The technique used for labeling is based on antigen-antibody coupling, which is a highly successful targeting method used in the human body. Each substance needs a specific approach with different capture particles and methods. This makes biosensors and the processes that allow them to function, an active field of study.

After the target has been captured, it has to be detected and the amount has to be measured in order to give diagnostic results. Biosensors use a variety of methods to detect the target, for example [2]:

- *Mechanical*
  Methods in this category use the physical weight of the target particles to detect them and measure the amount. Once the targets bind to the detector surface, properties of the mechanical probe are changed. The frequency of a vibrating crystal can change or the deflection of a cantilever can be enlarged. Measuring these changes can be a measure for the amount of target substance.
- *Electrical*
  Detection using electrical methods can be done using potentiometric, amperometric or conductometric properties of systems. In these systems, the target should either be charged itself or induce a reaction with products that are charged or involve electron exchange.
- *Optical*
  Measuring the target using optical methods involve a constant light source of which the light properties are known. Interaction of the light with the sample, or with surfaces in contact with the sample, leads to a change in the characteristics of the light falling onto a detector. The change in these characteristics from the original light source can be used as measure for the amount of target substance present in the sample.
- *Magnetic*
  By detecting changes in a magnetic field, the target substance can also be detected. Though, the target substances are mostly substances originating from the human body and these are generally not magnetically active. The magnetic methods are therefore used in sensors which use magnetic particles to label the target substance.

This report will not be concerning the detection, but rather the labeling of the target substance. The labeling involves the target being captured on mobile capture particles; the target particle binds to specific anti-bodies with which the capture particles are coated. Mobile capturing particles are used, rather than one stationary receptor surface, to enhance the speed of the capturing reaction (as a result of increased surface-to-volume ratio) and enable active transport. Active transport is enabled by capture particle characteristics, superparamagnetic in this case. Using a magnetic field, they can then be transported to a sensor surface. The surface is coated with specific anti-bodies onto which labeled target particles bind. When the gradient of the magnetic field is reversed, unbound capture particles are removed from the surface, while bound labeled targets remain at the surface. In biosensors using this capturing method, the amount of formed bonds on the surface, which is of course dependent on the amount of target particles present in the sample, can be measured using, for example, optical or electromagnetic effects. This measuring method is called a sandwich immunoassay (because the targets are "sandwiched" between an antibody on the capture particle and an antibody on the detector surface). This method is suitable for types of targets that exist only in small concentrations in the provided samples, because effectively, a double specificity is used, i.e. first in the target and the coating on the capture particle creating "antigen-antibody" pairs, and then in the binding of these pairs to the sensor surface. A schematic representation of this process using magnetic actuation is shown below in Figure 2.

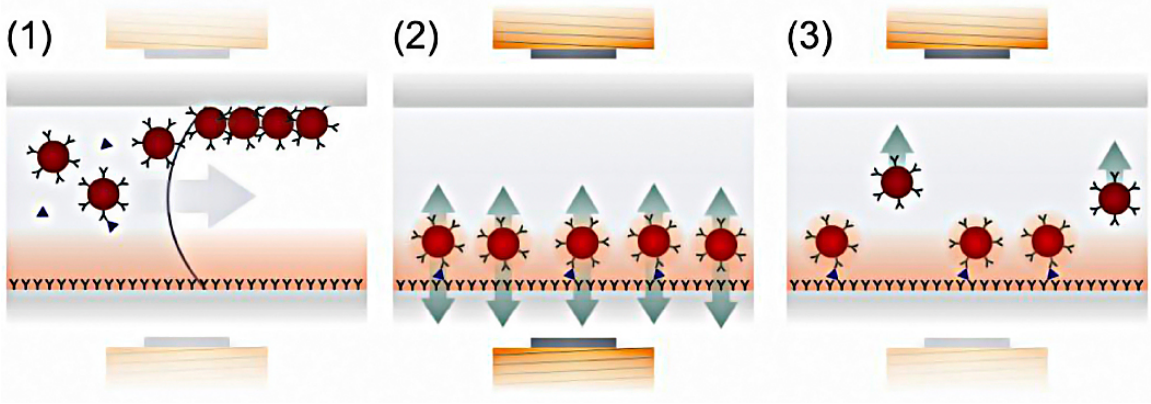

Figure 2: (1) The sample enters the sensor chamber and the capture particle diffuse into the sample. (2) All capture particles are moved to the sensor surface by means of a magnetic field, and the labeled target particles bind to the anti-bodies on the sensor surface (3) A reverse field is activated, removing the unbound capture particles from the surface, leaving only the bound target particles behind. A detection method is then used to determine the amount of labeled target particles, completing the sandwich immunoassay.

An example for an optical method is frustrated total internal reflection (FTIR). The system is schematically shown in Figure 3. A LED light source shines on the detector surface under such an angle that there is total reflection and that the camera receives the same intensity light as originates from the light source. At the plane of reflection, a small portion of the EM field leaks through to the opposite side, creating an evanescent EM field in the sample area. This field diminishes exponentially with the distance to the reflection plane. If the situation is such that the reflection plane is formed from two media, the evanescent wave does not transmit energy. However, if a third medium is introduced close to the reflection plane (in the order of a few wavelengths), some scattering of reflecting light occurs, resulting in less light being reflected to the camera. The labeling particles represent the third medium, so depending on the amount of target particles there are in the sample; more sandwich complexes are formed at the detector surface. This results in a decrease of reflected light intensity, which can be registered by the camera. These changes are then interpreted by software and the amount of bound labeled targets at the surface can be calculated.

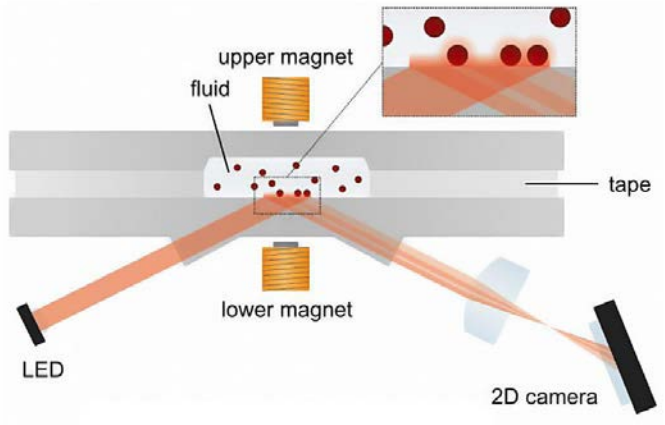

Figure 3: An optical detecting scheme using frustrated total internal reflection.

An example for applying electromagnetic effects in biosensors is using the giant magnetoresistance (GMR) effect. The method makes use of the magnetic properties of the superparamagnetic particles to detect them at the surface. A GMR sensor itself consists basically of 3 layers, the top and bottom layer being magnetically active (polarization changes under influence of magnetic fields) and a thin conductive layer in the middle. The top and bottom layer can change the conductivity of the middle layer as they react to external magnetic fields. The conductive properties of the middle layer can then be related to the amount of superparamagnetic particles at the surface.

The capturing of target particles with larger capture particles (labeling), described above as part of an sandwich immunoassay to determine target substance concentration, is the main subject in this report. The capturing process is as most reactions with multiple reactants, strongly dependent on the interaction between the capture particle and the target. This interaction may be influenced by characteristics of the surrounding environment, the buffer. Also, in research, some form of controlling agent is often used to create controllable and reproducible testing environments. To obtain usable test results, it is therefore important that those substances do not interfere with the studied interactions.

The research in this report focuses on analyzing the reaction kinetics of the capturing process (or, reaction) in different buffer conditions. The conditions that will be varied in experiments are the ionic strength (obtained by using a certain concentration of phosphate buffered saline, or PBS) and the concentration of bovine serum albumin (BSA), a protein used in many biochemical experiments to, among other applications, reduce non-specific binding of proteins. Also, the effect of agitation of the sample by vortex mixing on the reaction kinetics is studied.

The model sample will consist of fluorescent particles, which will act as the target particles, suspended in a PBS (phosphate buffered saline) solution. The use of fluorescent particles as target makes real-time tracking of the reaction possible and by recording the capturing reaction, the reaction kinetics of the capturing reaction can be studied using basic statistics. The employed capture particles are superparamagnetic particles. The capturing process will involve a streptavidin-biotin bond between the streptavidin coated, superparamagnetic particles and the biotin coated, fluorescent particles. The streptavidin-biotin bond is specifically chosen because streptavidin has a high affinity for biotin and they form one of the strongest non-covalent bonds in nature. This high affinity ensures that once a bond is formed, the chance of the bond breaking is small and this results in a high resistance of the bond to organic solvents, denaturants, detergents and extremes of temperature and pH.

2. Theory

In biosensors using labeling methods to detect the target, an important step is added to the detecting process. This step is the binding of target particles to labels, the capture particles. In the case studied here, superparamagnetic particles are used to catch the target. This capturing process can be described as a bimolecular process of which the kinetics can be described using standard reaction kinetics. In section 2.1, the kinetics of a bimolecular reaction will be expressed in general equations and important constants which characterize the reaction will be derived.

Also, to successfully label a target biomolecule, direct contact between the target and capturing (or labeling) particle has to be made. Before this, both particles register each other's presence through non-specific, remote interaction. In this report, the DLVO model is used to describe the interactions between particles with surface charge in liquid environments in the presence of ions. The model is explained in section 2.2.

2.1 Reaction kinetics

A bimolecular or two-component reaction in general is described as the encounter and association of two reactants, forming the reaction products. Not every encounter of reactants results in reaction products. The speed with which the reaction takes place is related to the rate of successful and unsuccessful reactions. This speed can be characterized by a reaction rate constant. The reaction rate constant is the main point of interest in most research done in reaction kinetics, because the speed of a reaction often determines the applicability of a process to the goal it is designed to achieve.

A reaction as described above can be schematically denoted as follows:[3]

$$A + B \underset{escape-encounter}{\longleftrightarrow} AB \underset{dissociation-formation}{\longleftrightarrow} C$$

To initiate a reaction, two reactants A and B, whose movement is governed by Brownian motion, must encounter each other. Upon encounter, they form a so-called encounter complex *AB*. This reaction intermediate can be transformed into the product C by a reaction specific process, or it can split up again into two separate reactants *A* + *B*. This second possibility is very relevant in binding proteins, as they most likely bind to specific proteins of another kind, such as in the streptavidin-biotin pair. The specificity is largely due to the shape of the proteins. If the alignment is not right, a bond is not likely to form. The last possible step in the reaction is dissociation, but considering the high affinity a specific protein pair has for each other, the possibility of that happening is considered negligible.

The rate at which this reaction takes place is expressed as the rate of change (time derivatives) in concentration of the reaction element in question, [*A*], [*B*], or [*C*]. The concentration [AB] is considered low (as is usually done for reaction intermediates) and in a steady state ($d[AB]/dt \approx 0$). This is the steady state approximation[4], and is used in a kinetic analysis of a complex reaction involving unstable intermediates in low concentration. The rate of change of each such intermediate is set equal to zero, so that the rate equation can be expressed as a function of the concentrations of chemical species present in measurable amounts.

Given an arbitrary multi-component reaction involving reactants/products *P*, *Q*, *R*, etcetera, the rate at which the concentration of a reaction element (say for instance, *P*) changes can be written using the rate law[5]. This law writes the rate as a product of the initial concentrations of participating substances (*Q*, *R*, and so on), and each is raised to an individual integer power (*m*, *n*, etc.) which represents the order of the reaction with respect to that reactant. This product is again multiplied by a reaction specific rate constant *k* (with units $M^{-1}s^{-1}$), i.e.

$$Rate = \pm \frac{d[P]}{dt} = k[Q]^m [R]^n \ldots \qquad (1)$$

The ± sign indicates that the reaction rate can be described from the standpoint of reactants (which gives a '-' as they are consumed), as well as products of the reaction (which then gives a '+', as they are produced). The overall reaction order is given by the sum of the exponents in (1). Zeroth-order reaction rates do not depend on the concentration of any substance. The first-order reaction rates can only depend on one concentration of substance involved. Second-order reaction rates can then depend on either one or two involved substance concentrations. An important to with respect to the reaction order, is that it is exclusively determined by experimental means and has no link to the stoichiometric notation of the reaction in a chemical equation[6].

The rate law stated in Equation (1) for the reaction scheme posed in the beginning of this section is developed as follows. First, the rate laws of all three possible steps are noted, followed by their individual rate law and definition of the reaction rate constant of the separate steps.

- $A + B \rightarrow AB,\ Rate = \frac{d[AB]}{dt} = k_{diff}[A][B],$

  $k_{encounter}$ = a diffusion rate constant, which brings A and B together
- $AB \rightarrow A + B,\ Rate = -\frac{d[AB]}{dt} = k_{diff'}[A][B],$

  k_{escape} = a diffusion rate constant, which diffuses A and B apart
- $AB \rightarrow C,\ Rate = \frac{d[C]}{dt} = k_{form}[AB],$

  k_{form} = a reaction rate constant at which C is formed from AB
- $C \rightarrow AB,\ Rate = \frac{d[AB]}{dt} = k_{diss}[C],$

  k_{diss} = a reaction rate constant at which C dissociates to AB

The diffusion rate constant is given in the Smoluchowski equation [7] as $k_{diff} = 4\pi DR$, with R the radius of the diffusing particle or sum of the radii of reacting particles. From the Einstein-Stokes equation[8] follows the diffusion coefficient $D = k_B T/6\pi\eta R$ with k_B the Boltzmann constant, T the temperature, η the viscosity and R again a particle radius or, D being the relative diffusion coefficient, in which case it is defined as the sum of diffusion coefficients of the reacting particles.

As stated earlier, [*AB*] is considered to be in a steady state. This can be said because the particles move in random directions in the medium (diffusion), and when they form an encounter complex, they either react or diffuse apart. The steady state formulated as $d[AB]/dt \approx 0$ can be in more detail by using rate laws above.

$$\frac{d[AB]}{dt} = k_{encounter}[A][B] - k_{escape}[AB] - k_{form}[AB] \approx 0 \rightarrow [AB] = \frac{k_{encounter}[A][B]}{k_{escape} + k_{form}}$$

The first term is positive, because the diffusion of *A* and *B* towards one another forms an encounter complex, increasing the amount of *AB*. The next two terms are then negative, because they decrease the amount of *AB* either by diffusion of *A* and *B* or by becoming a reaction product *C*. The rate of formation of the product C is then[3]

$$\frac{d[C]}{dt} \approx k_{form}[AB] = \frac{k_{form}k_{encounter}}{k_{escape} + k_{form}}[A][B] = k[A][B] \qquad (2)$$

The overall reaction rate constant k is thus a combination of the diffusion and formation rates, because all of these processes influence the effective reaction speed.

There are two limit cases for k[3], one in which $k_{escape} << k_{form}$ and one where $k_{escape} >> k_{form}$. If $k_{escape} << k_{form}$, then $k \approx k_{form}\, k_{encounter} / k_{form} = k_{encounter}$. In this case, the reaction is diffusion (or, transport) controlled. Typical values of (molecular) diffusion rate constants are in order of 10^9 $M^{-1}s^{-1}$ [9][10]. If $k_{escape} >> k_{form}$, then $k \approx k_{form}\, k_{encounter} / k_{escape}$. This represents a chemically-controlled reaction; the reaction rate constant is then reaction specific. For every reaction, the step from reaction intermediate to products has a different propensity to occur. This is expressed in equilibrium constants such as the association and dissociation constants, which are each other's inverse.

In this report, the interest lies with the binding reaction of two proteins, biotin and streptavidin, which have a high affinity for each other. They give one of the strongest non-covalent bindings in nature. This strength is expressed as a dissociation constant $k_d \approx 10^{-14}$ mol/l. The expression for this constant is $k_d = k_{dissociation} / k_{association}$, in which the association and dissociation are concerning the interaction between streptavidin and biotin.[10]

2.2 DLVO theory

Molecules are constructed from atoms and are held together by binding interactions such as covalent and ionic binding. In the first, an electron pair is formed that binds the two atoms together, in the latter, an electron is transferred, giving rise to an electrostatic binding. For molecules as a whole, and even larger particles, intermolecular interactions and bonds play a role, all of which are (actual reactions excluded) of a noncovalent nature.

Biological processes are dominated by noncovalent intermolecular interactions and bonds. These are mostly nonspecific, which means that they are present between almost any particle pair. The specific intermolecular bonds are much stronger, but these are again the result of a combination of multiple nonspecific interactions. These can become very complex when large molecules, or macromolecules, are involved. This complexity can be readily seen in biological processes in which certain proteins (macromolecules) target another macromolecule by having a specific shape which, in the right orientation, optimizes the nonspecific intermolecular interactions to form a strong intermolecular bond.[11]

In reactions, interactions between particles play an important role. To get a basic understanding of the reaction process, it is important to understand the remote interaction forces between the reacting particles that have either an attractive or repulsive effect and over what range they act. In this report, a model is needed to describe the interaction forces between particles with a surface charge, in a liquid medium containing ions. The model which does this is described in the DLVO theory, named after Derjaguin, Landau, Verwey and Overbeek. It describes the interaction between charged surfaces in a liquid medium. The description is based on the Van der Waals interaction (2.2.1) and electrostatic interactions due to the double layer effect (2.2.2), which is caused by the surface charge of the particles.[12]

2.2.1 The Van der Waals interaction

The Van der Waals interaction between particles is always present, even for totally neutral atoms and molecules. This force is the interaction between two particles at a certain distance, and is the sum of three components. The first component is the Keesom (or, orientation) interaction. This interaction force between two particles with a permanent charge distribution is either attractive or repulsive, according to the relative orientation.[12] The second component is the Debye (or, induction) interaction. This attractive force results from dipoles in one molecule, which induce a dipole in a second, non-polar molecule as a result of the electric field that the dipole causes.[12] The third and final component is the London (or, dispersion) interaction. Between any pair of molecules, whether they have (different) charge distributions or not, there is always an attractive force present.[12] Because this force is always present, regardless of the types of molecules involved, the London interaction force is important in many phenomena, such as adhesion and surface tension. The general Van der Waals interaction energy E_{vdw} can be expressed as [12]

$$E_{vdw}(r) = -\frac{C_{vdw}}{d^6} = -\frac{\left[C_{orientation} + C_{induction} + C_{dispersion}\right]}{d^6} \qquad (3)$$

with each C_i being specific for the situation at hand, depending on the involved molecules or particles and environmental parameters and d the distance between the particles.

This interaction energy is found in the interaction between two single particles. For the interaction between objects, some more definitions are needed. The interaction energy between objects in a certain environment is usually expressed in terms of situation specific distances and dimensions and a Hamaker constant A, which represents the properties of the objects and the surroundings. This constant is defined as [12]

$$A = \pi^2 C \rho_1 \rho_2 \tag{4}$$

with ρ_i being the number of atoms per unit volume and C the characteristic constant in the interaction energy. There are several theories on how to approximate these situation specific Hamaker constants, but in this report, assumed is that approximations found for different materials will be sufficient to obtain a decent model for the interaction energy.

For the interaction of objects in a medium, a total resulting Hamaker constant needs to be determined, which is defined as A_{1m2} (Hamaker constant A of interacting objects *1* and *2* in medium *m*). It is composed of A_{11}, A_{22} and A_{mm}, the Hamaker constants for each component interacting with another instance of itself in vacuum. The definition of A_{1m2} is then

$$A_{1m2} = c\left(\sqrt{A_{11}} - \sqrt{A_{mm}}\right)\left(\sqrt{A_{22}} - \sqrt{A_{mm}}\right) \tag{5}$$

The value c is dependent on the medium in which the interaction takes place. In this research the medium is water, for which c is defined as $c = 1.6$. [13]

The Van der Waals interaction between two spheres of different material and different radius R_1 and R_2 at a distance d is defined as (approximated by Derjaguin) [12]

$$E_{sphere-sphere,VdW}\left(R_1, R_2, d\right) = -\frac{A_{1m2}}{6}\frac{R_1 R_2}{\left(R_1 + R_2\right)d} \tag{6}$$

2.2.2 Electric double layer

The second interaction described in the DLVO theory is the electrostatic interaction. When a charged object is put in a liquid medium with ions present a so-called electric double layer will be formed due to shielding of the (surface-) charge of the object by ions of opposite charge. The first layer consists of ions with a charge opposite to the charge of the object, which are called counter ions. These ions are not bound, but rather adsorbed to the surface of the object and can be replaced by other ions of the same charge. This layer is called the Stern layer (which is considered to be situated half an ion diameter away from the surface). The second layer contains ions with the same charge as the first layer, but these are not at all attached to the object, but are situated loosely around the object. This layer shields off the potential of the object to zero, so the thickness of the layer varies with surface charge. Ions can freely diffuse in and out of this layer, though the total charge will remain approximately constant since an equilibrium is formed to minimize electrostatic energy. The effect of the double layer around the charged object is best visualized with the potential changing from $V_{surface}$ to V_0 in several steps caused by the different layers in the model. This is done in Figure 4. First, $V_{surface}$ is lowered almost linearly by the Stern layer to V_{Stern}. The next plane encountered is the shear plane, from there, the fluid can move freely around the object. The potential here is called the zeta potential, V_{zeta}. From here the potential exponentially decays to V_0, the potential of the bulk solution.[12]

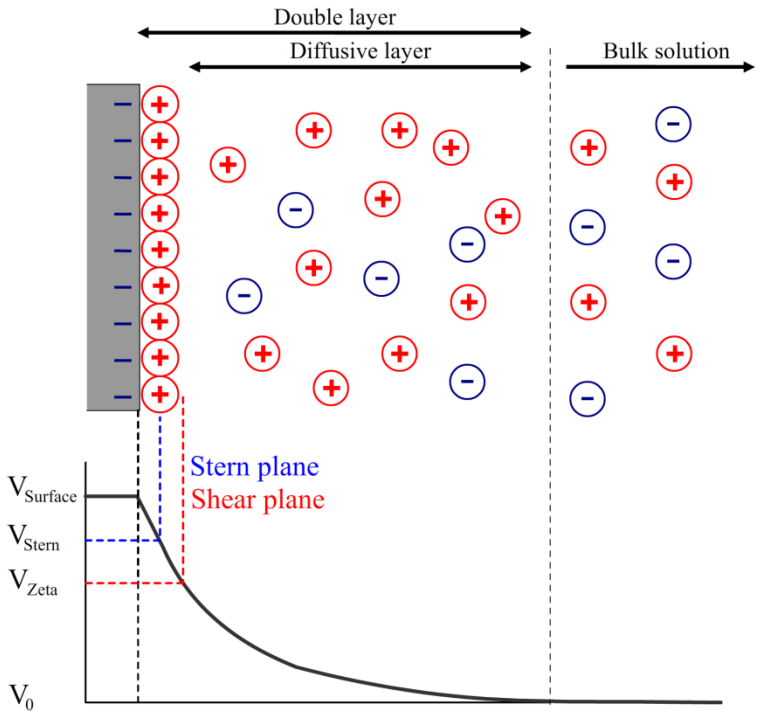

Figure 4: Schematic illustration of the electrostatic double layer interaction including the various components.

The electrostatic interaction between macromolecules or surfaces is described by a exponentially decaying function of distance between the interacting objects. It has the form $C \cdot \exp(-\kappa d)$, in which κ is the reciprocal Debye length and C a situation specific constant depending on object geometries and surface charges.[11] For two spherical objects, the electrostatic or double layer interaction energy, can be described as follows.

$$E_{sphere-sphere,Double-layer}(d) = C\exp(-\kappa d) = \frac{R_1 R_2}{R_1 + R_2} Z \exp(-\kappa d) \qquad (7)$$

The first term is to take the scale of the interacting particles into account. The constant Z is a constant based upon surface potentials of the particles ($V_{particle1/particle2}$), for which the zeta potential is used as approximation, mainly because this can be directly measured. The value for Z is calculated with

$$Z = 64\pi\left(\frac{k_B T}{e}\right)^2 \varepsilon_0 \varepsilon_r \tanh\left(\frac{zeV_{particle1}}{4k_B T}\right)\tanh\left(\frac{zeV_{particle2}}{4k_B T}\right) \qquad (8)$$

The constant z is the electrolyte valence of the medium (approximated in this report as $z = 1$, because only a negligible amount of ions has a valence of 2), κ is the Debye length, defined by

$$\kappa = \sqrt{\frac{2N_A e^2 I_c}{\varepsilon_0 \varepsilon_r k_B T}} \qquad (9)$$

is a function of material and environmental properties, with N_A the Avogadro constant, e the fundamental charge, ε_0 and ε_r the permittivity of vacuum and the medium in which particles 1 and 2 are suspended, respectively. Finally, there are the Boltzmann constant k_B, the absolute temperature T and I_c, the ionic strength of the medium, defined by a summation over all ion species in the medium with concentration c_i and valence z_i:

$$I_c = \frac{1}{2}\sum_i c_i z_i^{\,2} \qquad (10)$$

In the situations at hand in this report, the permittivity of the buffer ε_r is a situation specific constant. The solvent medium contains ions which have electromagnetic properties. Because they are present in a homogenous concentration, they can alter the permittivity of the solvent medium that forms the buffer environment. It is determined with the following formula.[14]

$$\varepsilon_r = \varepsilon_{solvent} - \delta_i c_i + b_i c_i^{\,3/2} \qquad (11)$$

The parameter $\varepsilon_{solvent}$ is the relative permittivity of pure solvent (78.45 for pure water), δ_i is the dielectric decrement for a specific ion species i and the parameter b_i describes the curvature of the dependence.

2.2.3 The Van der Waals interaction and double layer effect combined

The total DLVO interaction is a combination of the above mentioned Van der Waals interaction and the double layer effect. In Figure 5a below, a graphical representation is given on how the two interaction forces combine to a resulting total interaction energy curve, as function of distance between the interacting particles.

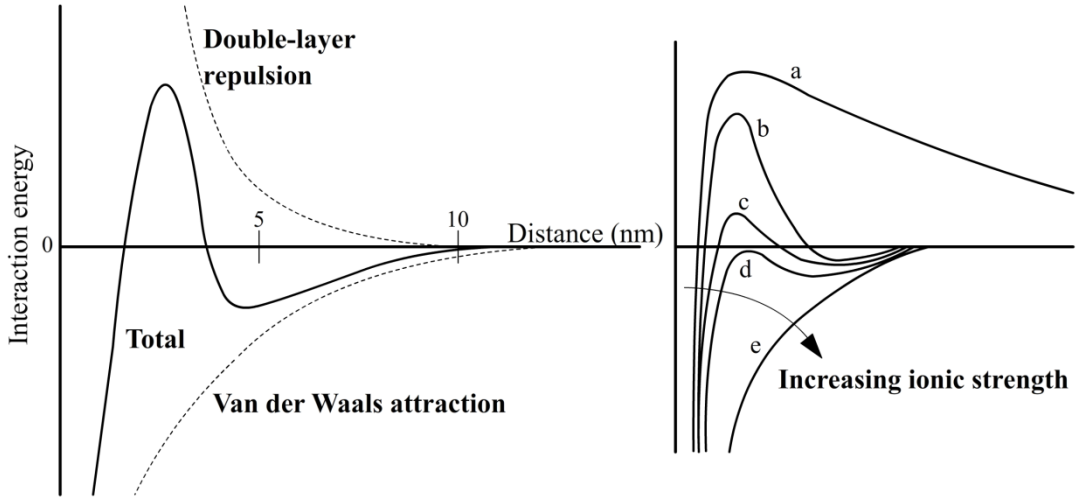

Figure 5a (left): The double layer and Van der Waals interaction combine to a total interaction energy curve between particles. (Note: the total interaction energy curve is only a general example) Figure 5b (right): The total interaction energy curve changes shape as the ionic strength of the medium surrounding the interacting particles changes.[12]

The Van der Waals force is the result of the correlation of dipole moments between molecules/particles and this interaction is not influenced by changes in ionic strength (or pH), this is an ever existing attractive force between the interacting particles. Also, it usually exceeds the double layer interaction at short distances. The Van der Waals interaction is proportional to $\sim 1/r^n$, growing increasingly as r approaches zero (when $r \approx 0$, depending on how r is defined, or at zero distance, the actual volume of the particles prevents them from reaching the infinite energy well of the $-1/r^n$ curve), while the double layer interaction force/energy has a definite value, depending on the specific surface charge. The interaction resulting from the double layer construction changes with the ionic strength of the medium, and consequently, the total interaction energy curve changes. In Figure 5b, a range of different situations is shown.

Curve (a) in Figure 5b gives the interaction in a dilute electrolyte (low ionic strength). It represents a strong repulsive force that acts over long distances. As ionic strength of the solution increases, the curve shows some other features. Apart from the primary minimum in interaction energy at distances approaching zero (direct contact, or a bond), a secondary minimum is created, separated from the primary minimum with an

energy barrier, as seen in curve (b). If the ionic strength of the solution is increased further, this energy barrier decreases, eventually pushing the energy barrier below E = 0 (set to the energy level reached asymptotically at large distances), as seen in curves (c) and (d) respectively. Further increasing the ionic strength gives an interaction curve that shows increasing resemblance to the Van der Waals interaction, as seen in curve (e).

3. Experimental setup

3.1 Target and capture particles

The particles that were used in this report are nano-sized fluorescent target particles and micro-sized superparamagnetic particles. The targets will be Invitrogen FluoSpheres® Fluorescent Microspheres (F8767) which will be captured by Dynal Biotech Dynaparticles® M-270 acting as the capture particle. The fluorescent particles have a diameter of 0.2 µm. These particles are made of polystyrene mixed with fluorescent dye and are coated with biotin and they have a zeta potential V_{zeta} = -22 mV (measured in PBS using a Malvern Zetasizer Nano). The excitation of the fluorescent dye is done with an mercury arc lamp, using the 488 nm spectral line. The Dynaparticles are polystyrene particles containing grains of magnetite, making the particles superparamagnetic. They are coated with a monolayer recombinant streptavidin covalently coupled to the surface and have a diameter of 2.8 µm. The particles are hydrophilic, and have a slight negative (surface) charge, and a zeta potential V_{zeta} = -15 mV (again measured in PBS using a Malvern Zetasizer Nano).

For both the superparamagnetic and the fluorescent particles, specific concentration formulas are specified in the product data sheet. The concentration of magnetic particles is defined as [15]

$$[MB] = \frac{6.7 \cdot 10^8}{N_A \cdot X} \cdot 10^3 \qquad (12)$$

with $6.7 \cdot 10^8$ being the number of particles per ml in the stock solution, X the used dilution (for example, X = 30 for a 30 times diluted solution), N_A the Avogadro number and 10^3 is a factor that ensures that the final value is in M (or mol/l). For the fluorescent particles, the concentration formula is the following [16]:

$$[FL] = \frac{6 \cdot C \cdot 10^{12}}{\rho \cdot \pi \cdot \phi^3 \cdot N_A \cdot X} \qquad (13)$$

Here, C is the stock concentration of the suspended particles (0.01 g/ml), ρ the density of polystyrene (1.05g/ml), φ the radius of the particles (1 µm), N_A the Avogadro number and X the used dilution factor.

The fluorescent particle concentrations that were used in the experiments were compared to the stock solution. This was to verify if the concentration did not differ from the intended levels. To determine this, fluorescence values of dilutions made from the supply for an experiment were compared to newly made dilutions in a fluorometer (Fluoroskan Ascent FL) and a correction factor was determined. These results are given in section 4.1.

3.2 Measurement setup

Measurements in the experiments are done with a Leica DM6000M microscope using lighting conditions such that both fluorescent particles and superparamagnetic particles were visible. The samples are placed under an immersion lens, and boxed in by an improvised screen to block external light, so that the sample was only illuminated by the mercury arc lamp. This activates the fluorescence in the fluorescent particles while also making the magnetic particles visible for the camera.

All analyzed samples consist of 0.5 µl superparamagnetic particle solution and 9 µl fluorescent particle solutions. The superparamagnetic and fluorescent particle solutions are placed in the encircled area in the

mentioned order, making sure to wait a few seconds to let the superparamagnetic particles settle before the fluorescent particles are added. The samples are put between two cover slips, held together by double-sided tape which encircled the sample area (Figure 6, with a cross section above and a top view below). The images were captured with an Andor Luca S EMCCD camera which was connected to a computer. The data collection was done with the Andor SOLIS software with which the images were stored for further analysis.

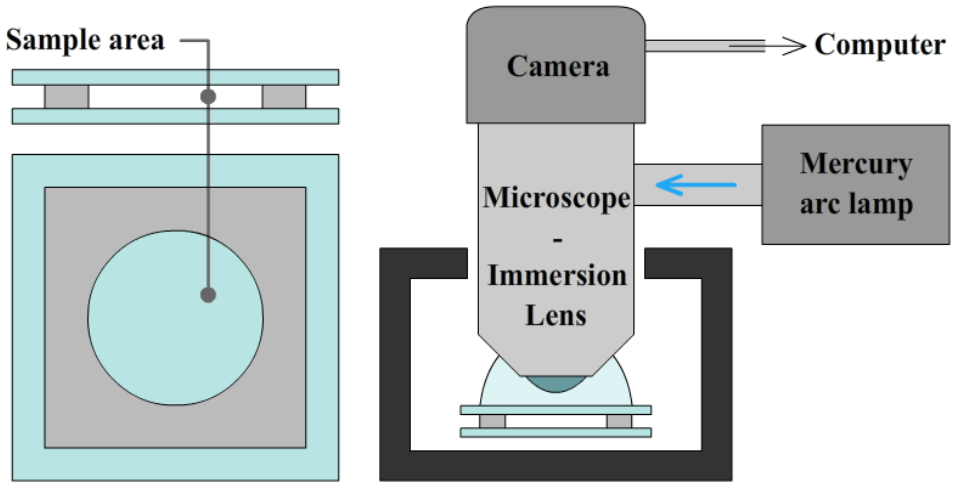

Figure 6: Left: Cover slip system for the analyzed samples. Above a cross section, below the top view. Right: The microscope setup.

3.3 Measuring binding events

Two methods of measuring binding events are used, of which each has its advantages and drawbacks. The fundamental difference between the two methods is the concentration of superparamagnetic particles. In this report, two particular dilutions are used: 30× and 200×.

In the experiments using a 30× dilution, a fixed location in the sample is chosen to analyze over time. The dilution of the superparamagnetic particles determines the amount of particles the field of view holds. When using this smaller dilution, the amount of particles in the field of view is between 40 and 50, ideally closely around 50. This location is then observed for half an hour and pictures are taken periodically. The number of fluorescent particles bound to superparamagnetic particles is then counted for each picture. From the results, the average amount of bonds per capture particle as a function of time is calculated. An example of an observed location is given below in Figure 7.

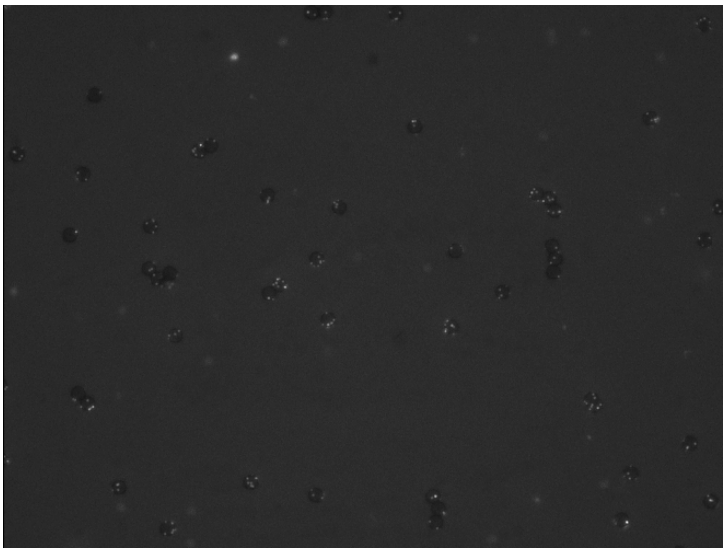

Figure 7: A location found in a sample using 30× diluted superparamagnetic particles and 3000× diluted fluorescent patricles. This examples shows 49 superparamagnetic particles with 179 fluorescent particles bound to the surfaces.

The advantages of this method are that the resulting curve can be very smooth, depending on how many measurements are done per unit of time, also resulting in a small standard deviation. This makes the curve convenient to be fitted with an appropriate function. The drawback of this method is that the target adsorption (the capturing process) of one superparamagnetic particle can influence the adsorption of a neighboring particle. Also, using these high particle concentrations, patches of even more than 50 particles per field of view can occur. This can cause the depletion of fluorescent particles to vary over the surface where the superparamagnetic particles are present. The influence the particles have on each other can be seen if the reaction rate constant for a reaction is compared at different particle concentrations. In Figure 8, taken from earlier experiments, the influence of the amount of superparamagnetic particles in a field of view is shown. It can be seen that with up to about 40 superparamagnetic particles in the field of view, the reaction rate constant is not influenced as much as with higher concentrations. As this is also the maximum amount of particles in the field of view that will be used in this report, expected is that no corrections will have to be made, though the results are still checked to determine if the influence is negligible or not. So, while fitting on the smooth curve leads to small uncertainties with respect to the measured values, the measured values themselves can have a high uncertainty which is hard to assess.

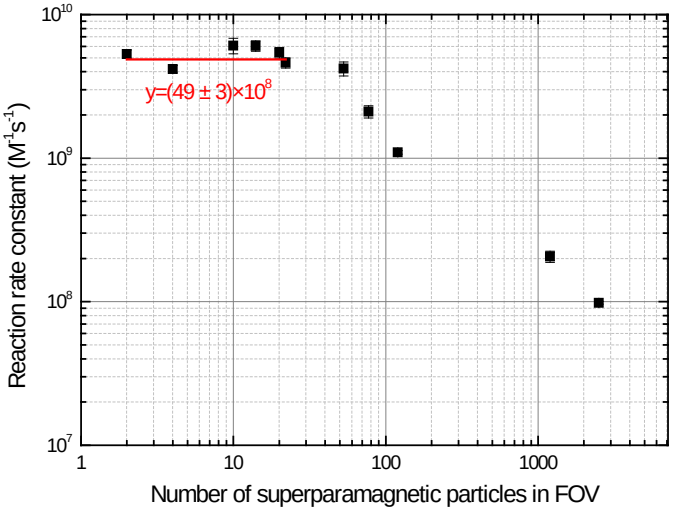

Figure 8: Reaction rate constant as function of number of particles in the field of view. The red line is a horizontal linear fit through the first 6 data points

For experiments using a 200× dilution, each time a photo is taken, a different FOV is set, which is approximately every 20 seconds. The superparamagnetic particle concentration is now so low, that every location contains only about one to five particles. For each picture, the amount of superparamagnetic particles and the number of fluorescent particles bound to a superparamagnetic particle are noted. The results are then put in a graph depicting the mean number of bounds per superparamagnetic particle as a function of time. An example of a typical field of view is given in Figure 9.

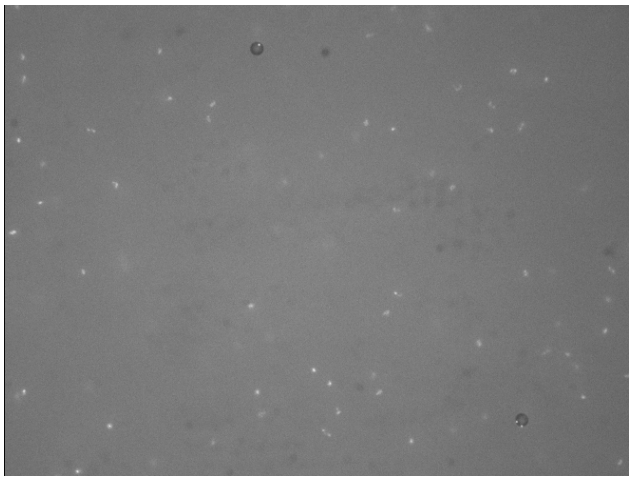

Figure 9: A location found in a sample using 200× diluted superparamagnetic particles and 3000× diluted fluorescent particles. This example shows three fluorescent particles bound on two superparamagnetic particles.

With this low concentration, the superparamagnetic particles are mostly far apart so that the particles do not influence each other's capturing of fluorescent particles. But, to get a smooth curve and low uncertainties, more observations have to be done to achieve good statistics. Also, more observations done means that more different particles are used in the measurement and that differences in local sample properties become less influential because more of the total sample area is taken into account.

3.4 Influence of ionic strength on the reaction rate constant

The energy barrier that has to be overcome in order to get a bond between a fluorescent particle and a magnetic particle is modeled by the DLVO theory. As the electrostatic barrier, one of the two components forming the total barrier, is influenced by ions present in the solution containing the sample, it may be possible that the capturing efficiency can be altered by changing the ionic strength of the solution. The efficiency is evaluated in the form of *k*, the reaction rate constant.

The experiments are done using the first method from section 3.3, using 30× diluted superparamagnetic particles and 3000× diluted fluorescent particles, taking a picture every two minutes for half an hour. For a measurement, 0.5 µl PBS (phosphate buffered saline, this salt solution determines the ionic strength) containing superparamagnetic particles is placed in a fluid cell, together with 9 µl fluorescent particles in a certain predetermined PBS concentration (0%, 1%, 10%, 33% or 100%). To reduce non-specific binding, 1% (10 g/l) BSA (Bovine Serum Albumin) is added to the PBS solutions. Every two minutes, a picture is taken and the number of fluorescent particles bound to magnetic particles is counted. From these results a time-dependent curve can be made from which the reaction rate constants can be determined using the theory described in section 2.1. A more detailed experiment protocol can be found in the appendix, section 7.1.

3.5 Influence of mixing on the capturing process

Some target substances exist in samples only in very low concentration. In these cases, relying on just diffusion to take care of the capturing process may not be enough, as the measurement time will have to be very long before retrieving adequate results. This is not compliant with the point-of-care requirements that a biosensor has to fulfill. A common solution to enhance the speed at which low concentration reactions take place is mixing. This increases the transport of particles through the solution medium. The type of mixing action that is applied in this experiment is vortex mixing and is done with an Eppendorf Thermomixer Comfort multitube vortexer. Eppendorf tubes containing the samples stand upright in the mixer which moves them in a planar circular fashion at a set amount of rotations per minute.

In this experiment a sample consists of 15 µl of 10^6× diluted fluorescent particles and 60 µl of 200× diluted superparamagnetic particles. To check whether the mixing improves the capturing process, three measurements are done in which the superparamagnetic particles are diluted using solutions of 0%, 10% and 100% PBS. The samples were put on a mixer which mixed continuously. The Thermomixer is set to room temperature and mixes the batch of sample tubes 1200 rpm. The samples are analyzed after spending roughly 5, 15, 50, 200 and 350 minutes on the mixer.

With each analysis, a small amount of the sample was taken and inspected with the microscope. Before analysis, a small magnet is held underneath the cover slips that contain the sample. This makes analysis of more capture particles possible, but also results in an irregular capture particle count in the analyzed FOV. Each time, five pictures are taken. Of each picture, the amount of superparamagnetic particles in the field of view was counted, and the number of fluorescent particles that are captured. What is looked for in the results of this experiment is whether a clear capturing process is taking place at the low concentrations that are used.

3.6 Influence of BSA on the capturing process

A problem faced in observing and analyzing specific reactions or processes in biological environments is the occurrence of non-specific binding of reactants to the surface of lab equipment. Reactants may be lost to surfaces which may lead to significant changes in concentration. Also, specific reactions between a protein-protein couple take place partly because of a certain compatibility between them, but if these proteins also undergo non-specific interactions with equipment surfaces or with other protein species in the environment, the reaction efficiency may be diminished greatly and lead to faulty measurements.

A common agent that is used to reduce non-specific protein reactions is itself a protein, called Bovine Serum Albumin (or, BSA). It is used in many biochemical applications, stabilizing enzymes and preventing adhesion (or, non-specific binding) to surfaces, usually without interfering with reactions. It is therefore

useful to see if the BSA influences the reaction studied in this report, the binding of biotin coated particles to particles coated with streptavidin. A fixed magnetic and fluorescent particle concentration is put together in a sample using the same sample method as in section 3.1. The solution in which they are suspended is 100% PBS with a varying concentration of BSA added to see if the presence of BSA changes the catching efficiency.

The first series of measurements were done with the first method described in section 3.3 (30× diluted superparamagnetic particles and 3000× diluted fluorescent particles), taking pictures every 20 or 30 seconds over a time period of half an hour. The BSA solutions that were studied were 0.1% (1 g/l), 1% (10 g/l) and 5% (50 g/l).

The second series used the second method from section 3.3, 200× diluted superparamagnetic particles and 3000× diluted fluorescent particles and pictures were taken every 20 seconds or so for a period of about 40 minutes. The same BSA concentrations were studied and the samples were analyzed using the second method from section 3.3. An important note: the fluorescent particles in this measurement are not the FluoSpheres® used in other experiments, but custom carboxyl biotinylated fluorescent particles (with the same fluorescent properties). This has no further consequences, as the measurements in this series are only compared among themselves and have no links to other measurements.

4. Results

4.1 Fluorescent particle concentration correction factor

As fluorescent particles are transferred and diluted before use in experiments, it is possible that a small fraction of particles binds non-specifically to the surface of lab equipment. This can lead to a decrease in actual fluorescent particle concentration, even more so when the solutions are stored for longer time before being used. Therefore experiments were performed to check whether the concentration of fluorescent particles had decreased, and if so, by how much. To take this effect into account, a correction factor for the fluorescent particle concentration is determined.

For the experiment described in section 3.4, a 100× diluted supply was made from the stock solution of fluorescent particles. From this supply, a series of dilutions was made. The same series was created from the stock solution to be used as reference. The fluorescence of both dilution series was measured using a Fluoroskan Ascent FL fluorometer. By comparing the results from both series, it could be determined if and if so, how much the concentration of fluorescent particles in the samples from the used supply has diminished. The results from the fluorometer are given in a graph in Figure 10.

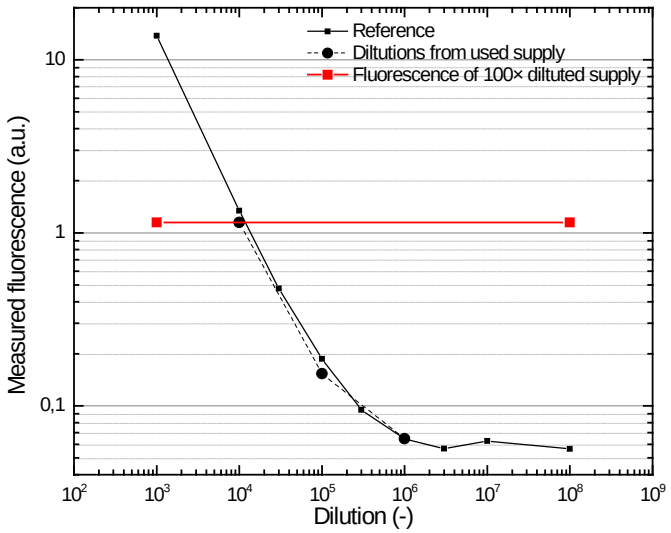

Figure 10: The graph shows the fluorescence measurements. The black curve gives the fluorescence intensity (in arbitrary units) of the reference dilutions. The red line indicates the intensity level of the 10,000× dilution made from the supply. A slight deviation is immediately visible. The fluorescence intensity of the 10,000× dilution from stock is higher than the same dilution made from the 100× diluted supply made earlier.

As fluorescence should be linearly proportional to the concentration (at low concentrations) of the fluorescent substance, it can be seen that the readings from samples with dilutions greater than 100,000× deviate from this behavior. With dilutions exceeding $1 \cdot 10^6$×, the intensities of the reference curve are beneath the sensitivity of the fluorometer.

The curve of measured intensity values from the 100× diluted supply shows lower intensity values than the reference curve. It can therefore be concluded that the fluorescent particle concentration, has indeed decreased during the handling and storage of the solutions.

The change in concentration is determined using the intercept of the fluorescence level of the 10,000× dilution from the used supply solution with the reference curve. It is determined that the measured fluorescence of the 10,000× dilution from the supply is 1.146±0.05 (error estimated, 0.05 is an error of approximately 4%). From the fit of the reference curve it is found that this value of fluorescence is actually achieved at a dilution of x = (12005±524)× dilution. The correction factor for the concentration therefore is 12005/10000 = (1.2±0.05), which is not considered negligible. More detailed calculations can be found in Appendix I.

The correction factor shows that samples that have spent more time in the Eppendorf tubes have a decreased concentration of fluorescent particles compared to the reference samples. The reference samples were made only minutes before the comparison, while the supply of 100× dilution spent several weeks in the tubes. The reasons for this deviation in fluorescent particle concentration could be that mistakes were made in preparing the original 100× dilution or that particles are lost to the surface of the tubes.

4.2 Influence of ionic strength on the reaction rate constant

The interaction between the superparamagnetic and the fluorescent particles is described by the DLVO theory (section 2.2). One of the components of the interaction, the electrostatic double layer effect, involves the influence of ions present in the buffer solution. It is therefore possible that varying ion concentration, or ionic strength, results in varying efficiencies of the capturing process, the reaction rate constant being a measure for the efficiency.

This was studied by varying the ionic strength using 5 different PBS concentrations. For each measurement, a fixed concentration of superparamagnetic and fluorescent particles was used. The superparamagnetic particles were suspended in pure PBS, while the fluorescent particles were suspended in the varying PBS dilution. The used PBS solutions are 0% (DI water), 1% (100× diluted), 10% (10× diluted), 33% (3× diluted) and 100% (pure PBS). This results in samples containing a total percentage of 5.26%, 6.21%, 14.74%, 36.84%, and 100% PBS, respectively. For each measurement, the formed bonds between fluorescent and superparamagnetic particles were counted as a function of time. The reaction rate constant could then be abstracted from fitted functions. The results for the measurements are plotted in Figure 11 below.

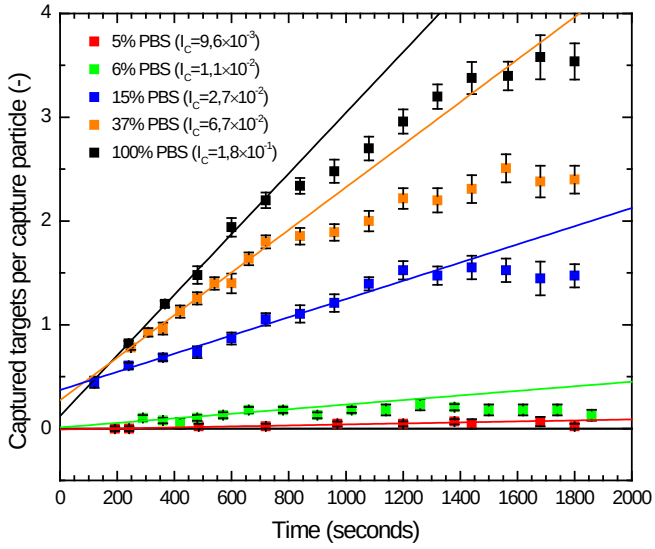

Figure 11: This graph shows the observed capturing events per capture particle as function of time, in solutions of varying ionic strength. Linear fits were made through the first few linear points, which were chosen at best insight. From these linear fits, the reaction rate constants can be determined.

The expression for the reaction rate of the formation of bonds [*FLMB*] is given (conform to the general expression in (2) in section 2.1) by

$$\frac{d[FLMB]}{dt} = k[FL][MB] \tag{14}$$

in which [*FL*] is the concentration of fluorescent particles, [*MB*] the concentration of magnetic particles and [*FLMB*] the concentration of bonds formed (the number of captured fluorescent particles in the analyzed field of view). To determine the value for *k*, the initial semi-linear increase at small time values is fitted linearly. The slope of each fit is directly represented as the left-hand term in equation (14). As [*MB*] and [*FL*] are known and regarded as approximately constant, *k* can be calculated from the linear fit. Noted should be that in analyzing the photos taken are from above, so only the top half of the capture particles can be observed. As a result, the value for [*MB*] has to be replaced by 0.5·[*MB*].

$$\frac{d[FLMB]}{dt} = slope = k[FL](0.5 \cdot [MB]) \rightarrow k = \frac{2 \cdot slope}{[FL][MB]} \tag{15}$$

In this formula, [*FL*] and [*MB*] are calculated with the concentration formulas given in (12) and (13) in section 3.2. The correction value for [*FL*] (calculated in section 4.1) is already taken into account in the results. The resulting *k* values are plotted in Figure 12.

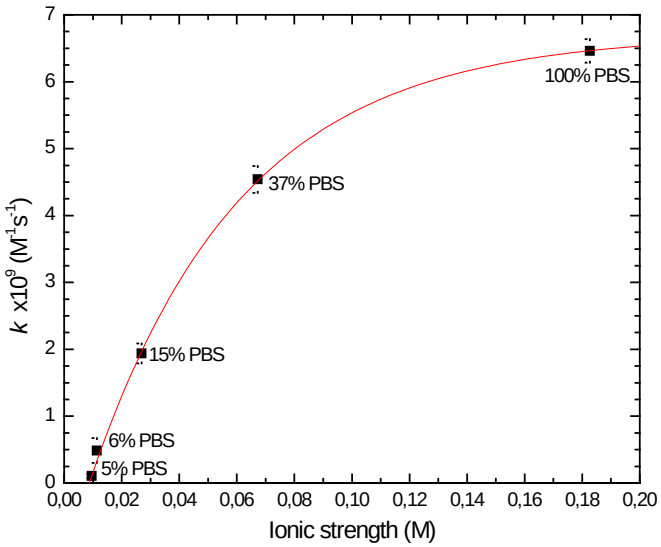

Figure 12: Value of reaction rate constant k as function of ionic strength. The values are fitted with an exponential function $y(x) = A\left[1 - e^{-B(x-C)}\right]$

The first thing that can be concluded from Figure 11 is that the presence of ions improves the capturing process. As the ionic strength of the buffer increases, the slope of the initial linear curve increases and with that, the value for *k*. The found values for *k* are fitted with an $y(x) = A\left[1 - e^{-B(x-C)}\right]$ function (the red line in Figure 12). This curve asymptotically approaches the limit $A=(6.7\pm0.2)\cdot10^9$ $M^{-1}s^{-1}$ as the ionic strength approaches infinity. This is of course only the theoretical limit, but it does imply that the maximum value for *k* is achieved by maximizing the ionic strength of the buffer. The reaction rate constant for in standard PBS conditions is $k = 6.45\cdot10^9$ $M^{-1}s^{-1}$ which differs only about 4% from the theoretical limit reached by the fitted curve.

It appears that higher ionic strengths are favorable to the capturing process. This can be attributed to reduction in the repulsive interactions between the fluorescent and superparamagnetic particles. The ions in the solution shield the surface charges of both the fluorescent as the superparamagnetic particles. This leads to a decrease in the electrostatic repulsive interaction and this will make it easier for the fluorescent particles to approach the capture particles. The capturing only takes place if the proteins on both particles approach each other in the orientation which maximizes the assembly of non-specific intermolecular interactions, and encounters will be easier and thus occur more frequently if the repulsive interactions between the fluorescent particles and superparamagnetic particles has been diminished, in this case using the enhanced shielding in higher ionic strength conditions.

The two bottom curves of Figure 11 (for 0% and 1% PBS) do not show the same distinct behavior as the curves measured with the higher values of PBS concentration, the values remain very close to zero. No increasing number of counted capturing events is visible. The capturing events that do occur could then also be interpreted as random and to be bound with only non-specific intermolecular interactions. Then the bottom curves would not represent the reaction that is obviously present with higher PBS concentrations, judging by the shape of the other data curves. These bottom curves will not only give high relative uncertainty in the slope of the linear fit through the first few data points due to the near-horizontal shape, but can also pose the question whether there is still protein activity in these conditions. To verify this, another form of actuation is examined, namely vortex mixing.

4.3 Influence of mixing on the capturing process

At low target concentrations, it may be gainful to improve transport of particles through the sample by means of mixing. Three samples containing the same target and capture particle concentrations but different concentrations of PBS are put on a multitube vortexer and periodically analyzed under the microscope using the second method described in section 3.3. The results are given in Figure 13.

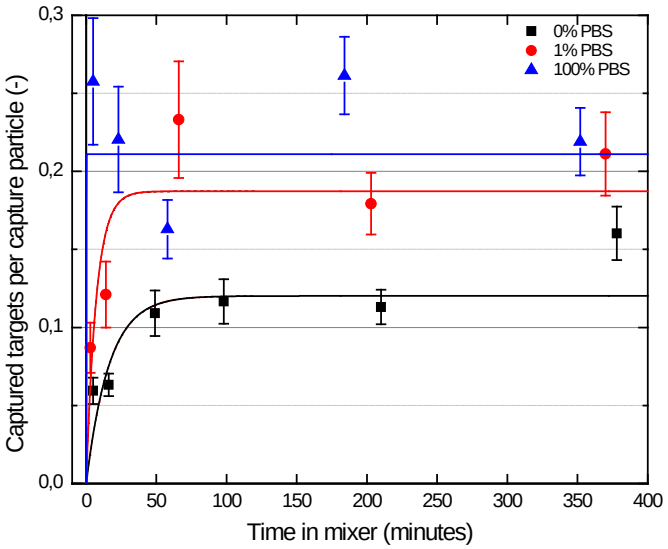

Figure 13: Average captured fluorescent particles per superparamagnetic particle as function of time spent in the mixer.

The results show a similar shape as in Figure 11 in section 4.2 though not as distinct, some data points clearly differ from the expected curve. The fits are of the form $y(x) = A\left[1 - e^{-Bx}\right]$ (derived in more detail in Appendix II), The horizontal parts may have a large error because of the behavior of the data points. These do not display the type of exponential behavior with which they are fitted.

The 100% PBS curve reaches its saturation point the quickest, just as in the previous experiment. The initial slope of the curves is again steeper as the ionic strength of the buffer is higher. The saturation levels are ranked in the same order as the initial slope, curves measured at higher ionic strengths saturating at higher levels. The data points do not show a clear correspondence to the fitted curves, with data points appearing well above or below the curve, in some cases even omitting the fits from their vertical uncertainty range. This is most likely the result of insufficient statistics. Every data point is the average taken over five or six pictures. In each picture, the number of capture particles in the FOV (ranging from about 20 to 100) and the number of bound target particles are counted, and uncertainties of the counts are estimated. The values captured targets per capture particle are then averaged for each sample, which are the data points plotted in Figure 13.

As the concentration of fluorescent particles was very low, and the method of measuring also used the high dilution of superparamagnetic particles (200×), the results may have been better if for each time interval, more pictures were taken, and maybe at more moments in time. Also, it is assumed that the mixing process does not break the strong streptavidin-biotin bonds. Otherwise, it is expected that the results show less correlation in relation to ionic strength. While bonds are more easily formed in high ionic strength conditions, the bond remains as strong in 100% PBS as it is in DI water.

What can be concluded from Figure 13 is that a bond between the streptavidin and biotin on the particles is still possible at 0% PBS, because the curve shows the expected behavior. This suggests that a binding process is taking place, however at a lower speed and efficiency than at higher values of ionic strength of

the solution. The mixing thus ensures that the two bottom curves in Figure 11 are still viable in the results, because there is shown that there is actual capturing activity.

To further examine the effects of the mixing process on the capturing process, reaction rate constants k_{mix} are determined from the exponential fits in Figure 13, by taking the value for parameter *B* and dividing it by the concentration of capture particles (for details, see Appendix II). The k_{mix} values are compared with the *k* values obtained using only diffusion as reaction actuation mechanism, the experiment of which the results are given in section 4.2. These *k* values are here labeled as k_{diff}. The comparison is done in the graph in Figure 14 where k_{mix} is plotted as function of k_{diff}.

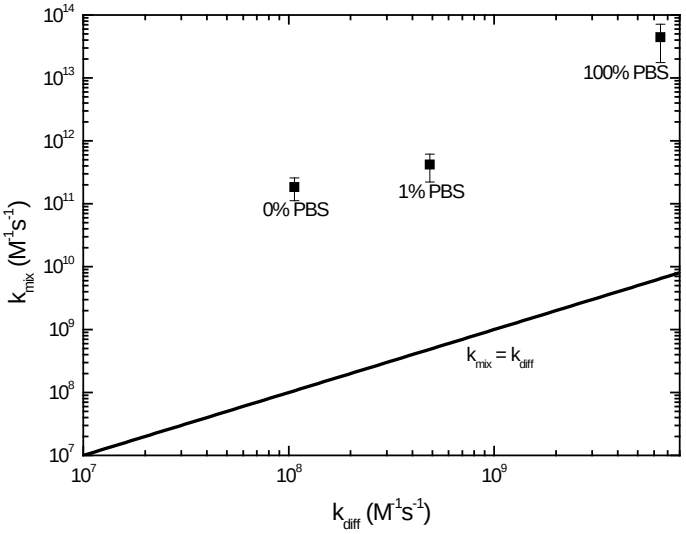

Figuur 14: Graph showing k_{mix} values as function of k_{diff} reaction rate constants. The line $k_{mix} = k_{diff}$ is plotted to conveniently show the improvement of the reaction rate constant by application of mixing.

In Figure 14 the line $k_{mix} = k_{diff}$ is shown. This makes it convenient to see that the reaction rate constant, and with that, the efficiency of the capturing process is enhanced by applying mixing to the sample, as all k_{mix} values are well above the $k_{mix} = k_{diff}$ line. The observed improvements are in the order of 10^4. Noted should be again the insufficient statistics visible in Figure 13 in the form of fluctuations around the saturation level and, for example, the first three data points of the 100% PBS measurement being declining instead of increasing. This can lead to overestimation of initial slopes of the fitted curves, especially in the case of the 100% PBS measurement. Concluded is still that a mixing protocol can be applied to samples with low concentration capture particles and/or targets to improve the capturing process. This is done by increasing particle transport through the medium, thereby increasing the collision frequency, theoretically resulting in more successful encounters per unit of time. Also, the mixing increases the kinetic energy of the particles, which, in some reactions, increases the chance that meeting particles overcome repulsive interactions and start a reaction. Further research is needed to determine whether this is the case in this experiment, or whether it is even necessary with the studied binding process.

4.4 Influence of BSA on the capturing process

In this experiment, the goal is to look whether BSA influences the streptavidin-biotin binding process that occurs with the capturing of fluorescent targets with the superparamagnetic particles. The fluorescent and superparamagnetic particles are both diluted in PBS and a certain amount of BSA is added. From a sample, the average amount of bonds per superparamagnetic particle is observed over time. Both of the two methods described in section 3.3 are used and the results will be given in that same order.

The results of measurements using the first method with 30× diluted superparamagnetic particles are given in Figure 15.

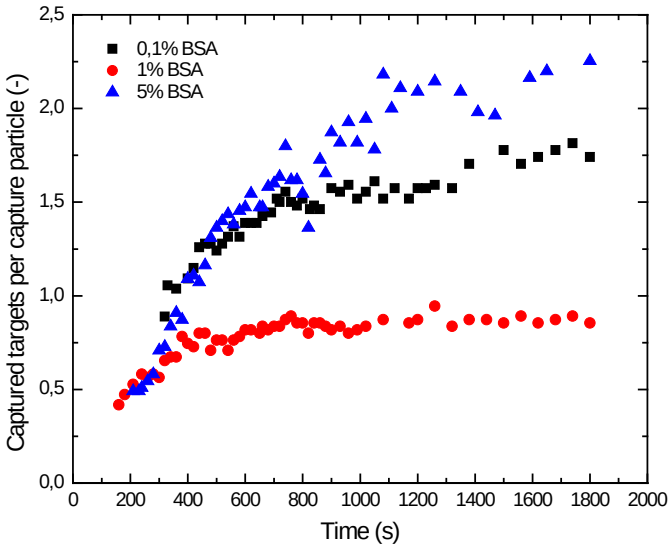

Figure 15: Graph showing the average captured fluorescent particles per superparamagnetic particle with varying BSA concentration, using 30× diluted superparamagnetic capture particles.

Three distinct curves are visible, all having the same shape as the curves in section 4.2. The curves do not seem to have a ranking order either in increasing or decreasing BSA concentration, starting from above with 5% BSA, followed by 0.1% and 1% as the lowest curve, neither in initial slope nor by the levels reached by the curves. Furthermore, the saturation levels are very low with only about 2 fluorescent particles captured per superparamagnetic particle. All the previous observations taken into account, it is not possible to draw any real conclusions from these data.

The inconsistent curves suggest that there is some factor in the measurements that went wrong. One factor in the measurements that could lead to inconclusive or even useless results is that the field of view is continuously illuminated by the light source used to invoke fluorescence in the target particles. This can for example lead to the heating of the sample in the field of view. Although, taking into account the streptavidin-biotin protein pair being specifically chosen for its high affinity, this may be negligible. Another effect of the excitation light could be that the proteins on the superparamagnetic capture particles undergo photo oxidation. The continuous illumination of the particle surface can photo oxidize certain groups in the streptavidin molecule which may result in a decrease in reactivity. The same can be said for the biotin coated fluorescent particles, although these can diffuse freely in and out of the field of view while the superparamagnetic particles are stationary.

For future experiments, these problems can be averted by blocking the light on the sample and only illuminating the field of view when taking pictures. In the course of these experiments however, it was first suspected to be the state of the fluorescent particles that were in stock. Therefore, a switch was made to custom carboxyl biotinylated fluorescent particles to rule out dysfunctional target particles and the measurement method was changed to the second method from section 3.3, thus using 200× diluted superparamagnetic particles and a different field of view for each picture that is taken. The subsequent results are given in Figure 16.

.

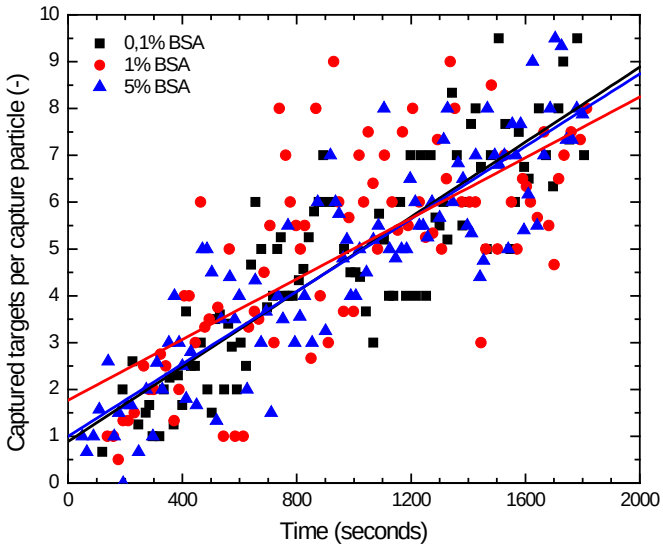

Figure 16: Graph showing the average captured fluorescent particles per superparamagnetic particle with varying BSA concentration, using the custom carboxyl biotinylated fluorescent particles.

Using a different method and different fluorescent particles seems to have a great effect on the results of the measurements. The curves now have the same distinct shape and the actual values do not differ among these measurements as they did with the previous ones. For every different BSA concentration, the slopes of the curves are very close to each other. This is also illustrated by the linear fits through the data.

The results from the first experiment suggest that a capturing reaction is taking place, judging by the consistent shape of the curves. However, no ranking order is found with respect to the BSA concentration but the curves are too dissimilar and inconsistent to draw any final conclusions. The second experiment again lacks any ranking order in BSA concentration, but the results now show more consistency while varying the BSA concentration. Taking the previous results into account, combined with the fact that BSA is widely used as stabilizing agent, it can be concluded that BSA also does not interfere with the capturing process studied in this report.

4.5 Model of the interaction energy

An attempt was made to create a simple model of the interaction energy curve by filling in the parameters of the formulas in sections 2.2.1 and 2.2.2 (the Van der Waals interaction and the double layer effect, respectively) and combining them as described in section 2.2.3. The Van der Waals interaction is constant as it is not influenced by the presence of ions in the surrounding medium. The double layer effect however, depends on the ionic properties of the medium and therefore has to be calculated separately for each different ionic strength value used in the experiment of section 3.2.

The Van der Waals interaction is defined (according to the Derjaguin approximation) in formula (6) in section 2.2.1. This contribution is crucial at short distances and thus, close to contact and/or binding. This is because of the *~1/d* dependence which becomes large at small distances between the particles. With the appropriate values inserted, it becomes

$$E_{sphere-sphere,VdW}(d) = -\frac{2{,}07 \cdot 10^{-28}}{d} \qquad (16)$$

The constant in the numerator is, as was found in plotting the curves, of great importance to the shape of the resulting interaction energy curve. It changes depending on the Hamaker constants that were used. These Hamaker constants are material specific, and since the objects in the system of the experiments are not homogenous, the actual Hamaker constants of the interacting particles will be combined, object specific Hamaker constants (not to be confused with (5), the total resulting Hamaker constant, which describes the system as a whole), which together, form the Hamaker constant for the total interaction. As only the total combined Hamaker constant is formulated in (5), estimations have to be made. Also, coefficient c in (5) is approximated with $c = 1.6$ (but is reported to have a value between 1.5 and 1.6) [17], which is actually for pure water, not ionic solutions.

The difficulty in approximating the Hamaker constant lies in the inhomogeneity of the interacting particles. There are interacting proteins, polystyrene and in one of the particles are embedded magnetite particles. For proteins, Hamaker constants are reported to be, for example, ~1.23–4.11·10^{-26} J in water (~3–10 kT, 1 kT = 4.11·10^{-27} J at 298.15 K)[18] and near 1–1.5·10^{-20} J (lower values for solutions with higher salt concentrations [19]. The total resulting Hamaker constant for the system lies in the orders ~10^{-28} – 10^{-27} (the higher order yielding more pronounced curve features), and changing the value for c from 1.6 to 1.5 lowers the Hamaker constant with about 6%.

For the double layer effect, some assumptions and approximations were made. In formula (11) in section 2.2.2, the concentration c_i and $\varepsilon_{solvent}$ are known, however, for the dielectric decrement δ_i, the only definitive values that could be found were for sodium, potassium and chlorine ions. For the other ions in PBS (hydrogen phosphate and di-hydrogen phosphate) estimates are made. The parameter b_i has been approximated with 1 for all ions. Modulating these values only gave visible (but still negligible) deviations when in the orders well beyond usual parameter values. For detailed information on the values of these and other parameters used in modeling the interactions, as well as the final curve formulas, see Appendix III. In Figure 17, the curves are plotted, showing only the secondary minimum (as described in 2.2.3).

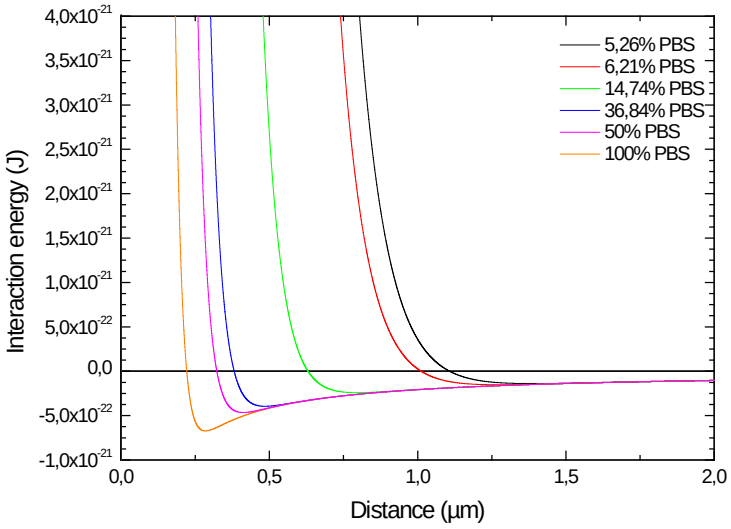

Figure 17: The five curves of total interaction energy at different ionic strengths, zoomed in on the secondary minimum.

Figure 17, depicting the secondary minimum at different PBS concentrations, clearly displays the behavior as described in section 2.2.3. The secondary minimum is increased when higher PBS concentrations are used, which indicated a decrease in the repulsive interaction between the particles. This is because the higher amounts of ions present shield the surface potential of the interacting target and capture particles more efficiently. This decrease in repulsive interaction allows the fluorescent particles to be captured by superparamagnetic particles more easily.

5. Conclusions

As a model for the labeling process in biosensors, the capturing process of biotin coated, nano-sized, fluorescent particles (targets) by streptavidin coated, micro-sized, superparamagnetic capture particles was introduced. The goal was to study how the capturing process is influenced by various buffer conditions, looking at ionic strength and the presence of BSA. Also, vortex mixing was tested as a form of actuation for the capturing process.

First, the influence of the ionic strength of the solution was studied, which is regulated by changing the PBS concentration. The initial results show that when the PBS concentration is increased, the curves rise more rapidly at the beginning and seem to settle at a higher amount of targets bound on the capture particles. The increasing slope indicates an increasing reaction rate constant, which leads to the conclusion that the presence of ions in the buffer leads to a more efficient binding process between the particles. This improvement in efficiency is attributed to the double layer effect, the electrostatic contribution to the DLVO interaction. Both the fluorescent and superparamagnetic particles have a negative surface charge, which will attract ions of opposite charge. This will shield off the potential caused by the charge and will decrease the repulsive force between the two particles. The height at which the curves settle seems to vary with the PBS concentration, but this is not conclusively shown with these graphs because the experiments were limited to run only up to 30 minutes. Due to the positive effect the increasing ionic strength has on the capturing process, the curves from experiments with lower ionic strength will take more time to get to the same saturation level as the curves measured at higher ion concentrations. The height at which a curve of this reaction in general levels out is when the maximum amount of fluorescent particles has bound to the superparamagnetic particles, or when the target particles run out.

The reaction rate constants determined from the results, plotted as function of ionic strength show a good correlation with the exponential function fitted through them. The exponential function asymptotically reaches a maximum value, but only at an ionic strength that goes to infinity. This limit is purely theoretical and cannot be reached, as the buffer liquid gets saturated at some point. However, the maximum ionic strength that was tested (buffer solution is then pure PBS) approaches the theoretical limit to within 96% of that value.

There is, however, a drawback in optimizing the shielding of surface potentials. Not only the capturing process is favored by this effect, also non-specific binding processes gain efficiency. So, an optimum has to be found in the shielding of surface potentials by varying ionic strength, it should benefit the intended process while not letting the non-specific processes cause too much noise in the measurement results.

When examining the cases of 0% and 1% PBS, there appeared to be very little capturing activity. The exponential characteristics that were displayed by the higher PBS concentration did not present themselves. The number of captured particles per superparamagnetic particle remained low and did not seem to saturate over time. This may lead to the question if there is actually a capturing process taking place.

This question is answered in the second experiment, in which the influence of mixing on the capturing process is studied. The results show definite activity and the resulting curves are fitted with an exponential. The fit illustrates there is still an actual capturing process taking place, with a decreasing slope that finally settles on a saturation level. Again, the reaction has a higher efficiency in 100% PBS conditions, but there is still a definite reaction taking place in 0% PBS. The fits show however a varying saturation level, but this is most likely caused by the low quality of the statistics and uncertainty in some data points.

The reaction rate constants from the mixing experiment are then compared to the values of the diffusion driven experiment examining the effects of varying ionic strength. A plot is made, showing the reaction rate constants of the mixing experiment as function of the values obtained in the experiment in which ionic strength is varied. In all three cases of PBS concentration, a considerable increase of reaction rate constant is seen when mixing is applied. Considering the wide application of mixing to improve reaction speed and efficiency, it can be concluded that mixing could be helpful when analyzing samples with low concentrations of targets and/or capture particles.

The influence of BSA on the biotin-streptavidin bond based capturing process should be minimal or non-existent if BSA keeps its general behavior of non-interfering stabilizing agent. It was already added to the first experiment, so it is useful to see if the presence of BSA influences the results in any way. This does not seem to be the case, based on the results from the measurements done with 30× diluted superparamagnetic particles, analyzing a single FOV over time. The curves lack any ranking order with respect to BSA concentration and they show the same distinct behavior as the results from the PBS experiment. There is, however, still a difference in initial slope and the levels reached by the curves, while the experiment was done in a 100% PBS environment for all measurements.

The saturation levels reached by the curves are also very low, so in combination with the results being inconclusive, two factors in the experiment are changed. Firstly, the original biotin coated Invitrogen FluoSpheres are replaced by custom carboxyl biotinylated FluoSpheres to rule out dysfunctional target particles. The second change is that another measurement method is used, using 200× diluted capture particles and taking a different FOV per measurement, to rule out optical effects such as heating and photo oxidization of proteins on the surface of both target and capture particles.

With these changes the results look a lot more conclusive. Again, no ranking order is found with respect to BSA concentration, but, more importantly, the curves now show much more resemblance to each other, both in initial slope as in the height of the curve. This suggests that the same capturing process is taking place with all three BSA concentrations, with very similar, if not, the same reaction kinetics. Also taken into account is the fact that BSA is widely used for its stabilizing, non-specific binding counteracting properties while not interfering with the relevant reaction. All this can lead to the conclusion that BSA does not influence or interfere with the capturing process of the fluorescent particles by the superparamagnetic particles.

The capturing process studied in this report acts as a model for the labeling process in biosensors that analyze samples in which the target substance exists only in small concentrations. To enhance the labeling process, buffer conditions may be changed (i.e. ionic strength, addition of stabilizing agents such as BSA). Or the sample may undergo certain pre-testing treatments such as mixing to increase substance transport through the sample, a method often applied in processes to increase reaction speed. Looking at the results that were collected in the research, it is obvious that buffer conditions can play an important role in the labeling step in the detection process in biosensors, and that they can be used even, to optimize the labeling. Increasing the reaction rate constant by adding ions to the sample results in enhanced speed at which the labeling, and thus, the entire process take place. Changing buffer conditions does not, ordinarily, change the sample size drastically, nor does it require implementing bulky components.

Increasing the speed of the measurement while retaining portability and not compromising specificity and selectivity, in some cases maybe even improving them by using agents such as BSA, can enable biosensors to fulfill stricter point-of-care requirements. Using the alteration of buffer conditions may even allow the detection and measurement of new target substances in biosensors that as of yet have not attained a point-of-care status.

6. References

[1] R.S. Freire, C.A. Pessoa, L.D. Mello, L.T. Kubota, *Direct Electron Transfer: An Approach for Electrochemical Biosensors with Higher Selectivity and Sensitivity*, J. Braz. Chem. Soc., Vol. 14, No. 2, 2003, 230-243

[2] F. Scheller, F. Schubert, *Biosensors*, Techniques and Instrumentation in Analytical Chemistry, Vol. 11, 1991

[3] D.F. Calef, J.M. Deutch, *Diffusion-Controlled Reactions*, Ann. Rev. Phys. Chem., Vol. 34, 1983, 493-524

[4] A.D. McNaught, IUPAC, *Compendium of Chemical Terminology (2nd edition)*, Blackwell Science, 1997

[5] J.W. Moore, C.L. Stanitski, P.C. Jurs, *Chemistry: The Molecular Science (4th edition)*, Cengage Learning, 2011

[6] M. Mortimer, P. Taylor, *Chemical Kinetics and Mechanism*: *Vol. 1*, Royal Society of Chemistry, 2002

[7] M. Schlosshauer, D. Baker, *A General Expression for Bimolecular Association Rates with Orientational Constraints*, J. Phys. Chem. B, Vol. 106, 2002, 12079-12083

[8] T.M. Nordlund, *Quantitative Understanding of Biosystems: An Introduction to Biophysics*, CRC Press, 2010

[9] K. Spitz, J. Moreno, *A Practical Guide to Groundwater and Solute Transport Modeling*, Wiley-Interscience, 1996

[10] N.M. Green, *Avidin*, in *Advances in Protein Chemistry* by C.F. Anfinsen, Vol. 29, 1975, 85-130

[11] D. Leckband, J. Israelachvili, *Intermolecular Forces in Biology*, Quart. Rev. Biophys., Vol. 34, 2001, 105-267

[12] J. Israelachvili, *Intermolecular & Surface Forces (2nd edition)*, Academic Press, Harcourt Brace & Company Publisher, 1991

[13] J. Visser, *On Hamaker Constants: A comparison between Hamaker constants and Lifshitz-Van der Waals constants*, Adv. Coll. Interf. Sci., Vol. 3, 1972, 331-363

[14] T. Vilariñio, M.E. Sastre de Vicente, *Theoretical Calculations of the Ionic Strength Dependence of the Ionic Product of Water Based on a Mean Spherical Approximation*, J. Sol. Chem., Vol. 26, No. 9, 1997, 833-846

[15] *Datasheet Dynaparticles M-270 Streptavidin*, Dynal Biotech ASA, 2004

[16] *Datasheet FluoSpheres Fluorescent Microspheres*, Invitrogen, 2005

[17] A.A. Busnaina, G.W. Gale, *Ultrasonic and Megasonic Particle Removal*, Precision Cleaning, Proceedings, April 1995, 347-360

[18] M. Lund, B. Jönsson, *A Mesoscopic Model for Protein-Protein Interactions in Solution*, Biophys. Journ., Vol. 85, 2003, 2940-2947

[19] A. Van Reenen, X.J.A. Janssen, L.J. van IJzendoorn, *Non-specific interaction of superparamagnetic particles on a glass surface in a rotating magnetic field*, Internship report, Technische Universiteit Eindhoven, 2008

Appendices

Appendix I – Fluorescent particle correction factor: Detailed calculations

To compare the dilutions of the 100× diluted supply to the reference dilutions, a fit of the form $y = a \cdot x^b$ is applied to the first 3 points of the reference curve (which are still within the device range) and determined at what dilution the fluorescence is the same value of that of the presumed 10,000× dilution from the used supply solution.

The reference curve yielded the fit

$$y = (a \pm S_a) \cdot x^b = (13757.33407 \pm 26.41146) \cdot x^{-1}.$$

Wanting to compare values at a certain value of dilution (on the x-axis), the fit was converted to

$$x = \frac{(13757.33407)}{y} \text{ with uncertainty}$$

$$S_x = \sqrt{\left(\frac{\partial x}{\partial a} S_a\right)^2 + \left(\frac{\partial x}{\partial y} S_y\right)} = \sqrt{\left(\frac{1}{y} S_a\right)^2 + \left(-\frac{13757.33407}{y^2} S_y\right)^2}.$$

The fluorescence value at 10,000× dilution from the supply is measured to be y = 1.146 ± 0.05 (estimated error).

This corresponds to a dilution of the reference of x = 13757.33407 / 1.146 = 12004.65451 with S_x = 524.2700903.

This leads to a correction factor of f = 12004.65451/10000=1.200465451, S_f = 524.00903/10000 = 0.0524.

Appendix II – Influence of mixing on the capturing process: Fit function

As in section 4.2, formula (14) is used as the starting point to find the reaction rate constant. It is equated to –d[*FL*]/dt, as the target concentration gets lower as they are captured by the superparamagnetic particles.

$$\frac{d[FLMB]}{dt} = k[FL][MB] = -\frac{d[FL]}{dt}$$

The differential equation that is solved is $\frac{d[FL]}{dt} = -k[FL][MB]$, with boundary conditions $[FL](t=0) = [FL]_0$ and $[FL](t \to \infty) = 0$.

The solution is $[FL](t) = [FL]_0 \exp(-k[MB]t)$. It relates to the amount of capture events as follows: $[FLMB] = [FL]_0 - [FL](t) = [FL]_0 \{1 - \exp(-k[MB]t)\}$

In the graph in Figure 13, amounts of captured targets are divided by the amount of capture particles, again, as in section 4.2, with the capture particle concentration divided by two because only the top half is observed. This all leads to a fitted function of the form

$$\frac{[FLMB]}{[MB]/2} = \frac{[FL]_0}{[MB]/2} \{1 - \exp(-k[MB]t)\} = A\{1 - \exp(Bt)\}$$

Appendix III – Model of the interaction energy: Parameter information

Parameters and constants used for modeling the double layer interaction.
R1 and R2 are the radii of the interacting particles.
[e]- *Estimate (various values tried, only abnormal changes in non-realistic orders yielded significant deviations)*

PBS percentage of sample	I_c	ε_r	κ	$z^{[e]}$	Z	$(R_1R_2/(R_1+R_2))*Z$
5.26%	$9{,}6\times10^{-3}$	78,45	10284599	1	8,90E-11	1,66E-17
6.21%	$1{,}1\times10^{-2}$	78,47	11170712	1	8,91E-11	1,66E-17
14.74%	$2{,}7\times10^{-2}$	78,62	17190360	1	8,92E-11	1,67E-17
36.84%	$6{,}7\times10^{-2}$	79,04	27108704	1	8,97E-11	1,67E-17
100%	$1{,}8\times10^{-1}$	80,27	44318806	1	9,11E-11	1,70E-17

Parameters to be used in equation (11) for determining the relative permittivity of the buffer.
[x] - *Found in* Dielectric and Electronic Properties of Biological Materials, *by R. Pethig (John Wiley & Sons Ltd, March 28, 1979)*
[e] - *Estimate (various values tried, only abnormal changes in non-realistic orders yielded significant deviations)*

Ion species	δ_i	b_i
Na^+	-8 [x]	1 [e]
Cl^-	-3 [x]	1 [e]
K^+	-8 [x]	1 [e]
HPO_4^{-2}	-3 [e]	1 [e]
$H2PO_4^{-1}$	-3 [e]	1 [e]

All these parameters result in the following curves:

PBS solution	**Plotted curve of Van der Waals and Double layer interaction combined**
5.26%	-2,07E-28*(1/x)+1,66E-17*exp(-10284599,3*x)
6.21%	-2,07E-28*(1/x)+1,66E-17*exp(-11170712*x)
14.74%	-2,07E-28*(1/x)+1,67E-17*exp(-17190359,9*x)
36.84%	-2,07E-28*(1/x)+1,67E-17*exp(-27108703,9*x)
50%	-2,07E-28*(1/x)+1,68E-17*exp(-31520433,97*x)
100%	-2,07E-28*(1/x)+1,70E-17*exp(-44318806,5*x)